Pergamon

PII S1359-6454(96)00200-5

Acta mater. Vol. 45, No. 2, pp. 611–622, 1997

Published by Elsevier Science Ltd

1359-6454/97 $17.00 + 0.00

COMPUTER SIMULATION OF GRAIN GROWTH USING A CONTINUUM FIELD MODEL

D. FAN and L.-Q. CHEN†

Department of Materials Science and Engineering, The Pennsylvania State University, University Park, PA 16802, U.S.A.

(Received 27 July 1995; accepted 20 May 1996)

Abstract—The kinetics of grain growth in two-dimensions (2-D) were investigated by computer simulations based on a continuum diffuse-interface field model. In this model, a polycrystalline microstructure is described by many orientation field variables whose temporal and spatial evolutions can be obtained by solving the time-dependent Ginzburg–Landau (TDGL) equations. It is found that the time dependence of average grain radius $\bar{R}$ follows the kinetic law: $\bar{R}_t^m - \bar{R}_0^m = kt$ with $m = 2.0$ in the scaling regime, in agreement with most of the previous simulation and theoretical results obtained using sharp-interface models. It is shown that the Louat's function provides a reasonable fit to the grain size distribution obtained from the simulation. In contrast to the general belief that 4- and 5-sided grains transform to 3-sided before their disappearance in 2-D grain growth, we found ample evidence that 4-sided and 5-sided grains may directly evolve to a region of disordered material, whose size is on the order of the grain boundary thickness and whose boundaries with neighbours are not well defined, and then disappear. The dependencies of grain growth kinetics on the computational cell size, the discretizing grid size, grain boundary width, as well as the number of field variables were critically examined. *Copyright © 1997 Acta Metallurgica Inc.*

1. INTRODUCTION

Extended defects in crystals, such as grain boundaries in polycrystals, are always associated with positive excess free energies, and therefore are thermodynamically unstable. As a result, grain growth in polycrystals will always take place to reduce the total grain boundary area, and thus the total grain boundary energy.

Grain growth, due to its importance in controlling the physical properties of a wide variety of materials, has been extensively investigated [1, 2]. It was shown that, in the so-called scaling regime, a microstructure reaches a steady state in which only the average size increases while the normalized size distribution is independent of time [3, 4]. Due to the difficulty of directly incorporating topological features into analytical theories of grain growth [5–7], there has been increasing interest in using computer simulations to study grain growth in single-phase materials. A variety of models have been proposed. These include boundary dynamics models [8–10], vertex models [11–13], Potts models [14–16], Voronoi tellselation [17, 18], and models based on mean-field theories [19–22]. A common feature of all these models is that all of them describe grain boundaries as sharp interfaces having zero thickness.

Very recently, we proposed a rather different model for grain growth, in which grain boundaries are assumed to be diffuse with finite thickness [23–26]. In this diffuse-interface model, a polycrystalline microstructure is described by many orientation field variables, which distinguish orientation differences of grains and which are continuous functions of spatial position and time. The total grain boundary energy of a microstructure is a function of the field variables and their gradients, analogous to the diffuse interface theory of Allen and Cahn [27] for antiphase domain boundaries (APBs) in ordered alloys. Therefore, we call this model a diffuse-interface field model. The temporal evolution of these field variables, and thus the microstructural evolution and grain growth kinetics, were described by the time-dependent Ginzburg–Landau (TDGL) equations. The preliminary results based on this model have been reported in previous short communications in the context of ordering dynamics of a system with a large number of non-conserved order parameters [23] and of grain growth [24].

One of the main objectives of this paper, then, is to give a more detailed account of the model and to investigate carefully the dependence of obtained grain growth kinetics on the size of computational cells and the number of orientation field variables. The second objective is to compare the grain growth kinetics obtained from this diffuse-interface model with those obtained from other models, in particular, from the popular Potts model. Furthermore, it is generally believed that 4- and 5-sided grains transform to 3-sided before their disappearance in 2-D grain

†To whom all correspondence should be addressed.

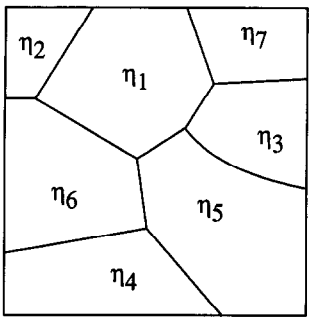

Fig. 1. A schematic microstructure described using orientation variables. The lines are grain boundaries.

growth. However, recent theoretical work on 2-D model systems by Fradkov [28] and experimental work on thin films by Palmer *et al.* [29] indicated that most of the grains remain in the same topological class until their disappearance. Therefore, the third objective is to examine, within the diffuse-interface description, the local topological changes of individual grains and to determine whether or not 4- and 5-sided grains must transform to 3-sided grains before their disappearance. The final objective is to examine critically the effect of grain boundary thickness as introduced in the diffuse-interface model on the kinetics of grain boundary migration.

2. THE DIFFUSE-INTERFACE FIELD MODEL

In the diffuse-interface field model, an arbitrary polycrystalline microstructure is described by a set of continuous field variables,

$$\eta_1(r), \eta_2(r), \ldots, \eta_p(r), \tag{1}$$

where η_i $(i = 1, \ldots, p)$ are called orientation field variables for distinguishing different orientations of grains and p is the number of possible orientations. A schematic microstructure represented by orientation fields in 2-D is shown in Fig. 1. For example, within the grain labelled by η_1, the value for η_1 is 1 while all other η_i for $i \neq 1$ is zero. Across the grain boundaries between the grain η_1 and its neighbour grains, the value of η_1 changes continuously from 1 to 0. The schematic profiles of η_1 and η_2 across the grain boundary between the grain η_1 and η_2 are shown in Fig. 2, all other field variables having zero values at and around this grain boundary. In real materials, the number of grain orientations is infinite, i.e. $p = \infty$. However, only a finite number of p can be modelled in a computer simulation. Therefore, the effect of the number of orientation field variables on the grain growth kinetics must be studied.

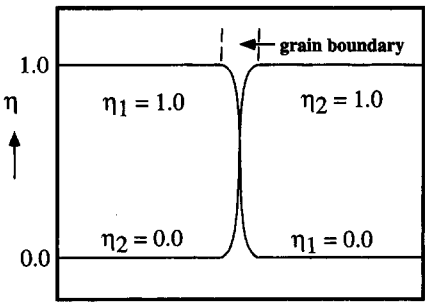

Fig. 2. The schematic profiles of two orientation variables across a flat grain boundary.

Similar to the treatment of APBs by Allen and Cahn [27], we write the total free energy of an inhomogeneous system in terms of all the orientation field variables and their gradients as:

$$F = \int\int\int \left[f_0(\eta_1(r), \eta_2(r), \ldots, \eta_p(r)) + \sum_{i=1}^{p} \frac{\kappa_i}{2} (\nabla \eta_i(r))^2 \right] \mathrm{d}^3 r \tag{2}$$

where f_0 is the local free energy density which is a function of field variables η_i, and κ_i are the gradient energy coefficients. The main requirement for f_0 is that it has p degenerate minima with equal depth, $f_{\min}$, located at $(\eta_1, \eta_2, \ldots, \eta_p) = (1, 0, \ldots, 0)$, $(0, 1, \ldots, 0), \ldots, (0, 0, \ldots, 1)$ in p-dimension space.

The origin of grain boundary energy comes from the gradient energy terms, $(\nabla \eta_i)^2$, which are non-zero only around the grain boundaries. According to Cahn and Hilliard [30], the energy σ_{gb} of a flat grain boundary between orientation i and j $(i \neq j)$ can be written as:

$$\sigma_{gb} = \int_{-\infty}^{+\infty} \left[f_0(0, 0, \ldots, \eta_i, \eta_j, 0, \ldots, 0) - f_{\min} + \frac{\kappa_i}{2} \left(\frac{\mathrm{d}\eta_i}{\mathrm{d}x} \right)^2 + \frac{\kappa_j}{2} \left(\frac{\mathrm{d}\eta_j}{\mathrm{d}x} \right)^2 \right] \mathrm{d}x. \tag{3}$$

It may be noted that the whole integrand is zero everywhere except at grain boundary regions. For a given f_0, the boundary energy and thickness vary with κ_i. The smaller the κ_i, the thinner the boundary region and the smaller the boundary energy. As will be discussed in more detail later, the only role of f_0 is to provide well-defined grain boundaries between different grains specified by the p degenerate potential wells since, according to the analysis of Allen and Cahn [27], in this diffuse-interface description, the boundary migration velocity is only proportional to the local mean curvature of the boundary and is independent of the potential function, f_0.

Since the orientation field variables are non-conserved quantities, their local evolution rates are linearly proportional to the variational derivative of the total free energy with respect to the local

orientation field variable, i.e. governed by Ginzburg–Landau equations,

$$\frac{\partial \eta_i(r,t)}{\partial t} = -L_i \frac{\delta F}{\delta \eta_i(r,t)}, \quad i = 1, 2, \ldots, p \quad (4)$$

where L_i are the relaxation coefficients, t is time, and F is total free energy. In the right-hand side of (4), the cross-terms have been assumed to be zero. The validity of this assumption remains to be verified. With $p = 1$, the Ginzburg–Landau equation has been extensively applied to modelling the dynamics of a quenched system with a non-conserved order parameter [31], to the kinetics of antiphase domain coarsening [27], and recently to solidification in a pure material [32].

3. MOTION BY MEAN CURVATURE

In traditional theories of interface motion, the boundary velocity, V, is generally written as

$$V = B\,\Delta\mu = B\sigma_{gb}\Omega(\lambda_1 + \lambda_2), \quad (5)$$

where B is mobility, $\Delta\mu$ is the chemical potential difference per atom across the boundary, σ_{gb} is the boundary energy, Ω is the atomic volume, and $(\lambda_1 + \lambda_2)$ is the mean curvature.

As mentioned above, if we set $p = 1$ and substitute the free energy expression (2) into the kinetic equation (4), we obtain the equation for the evolution for APBs described by the long-range order parameter field η,

$$\frac{\partial \eta(r,t)}{\partial t} = -L\left[\frac{\partial f_0(\eta)}{\partial \eta} - \kappa\nabla^2\eta\right]. \quad (6)$$

By assuming that the APB width is much smaller than the domain size, Allen and Cahn [27] showed that the APB migration velocity is given by:

$$V = L\kappa(\lambda_1 + \lambda_2). \quad (7)$$

The important implication of (7) is that APB motion is only determined by the local mean curvature and is independent of the specific form of the local free energy density function, f_0. It can be shown that for isotropic grain boundary energy and isotropic relaxation constants, a grain boundary within the diffuse-interface description also moves due to mean curvature and we obtained exactly the same equation for the boundary velocity as (7).

4. CONSTRUCTION OF THE LOCAL FREE ENERGY DENSITY

As pointed out in the last section, for the purpose of modelling grain growth in a pure system, the exact form of the free energy density function, f_0, is not important for the motion of APBs and grain boundaries. The only requirement for f_0 is that it provides large numbers of potential wells with equal well depth located at $(\eta_1, \eta_2, \ldots, \eta_p) = (1, 0, \ldots, 0)$, $(0, 1, \ldots, 0)$, $\ldots$, $(0, 0, \ldots, 1)$, respectively. A simple function which satisfies this requirement is

$$f_0(\eta_1, \eta_2, \ldots, \eta_p) = \sum_{i=1}^{p}\left(-\frac{\alpha}{2}\eta_i^2 + \frac{\beta}{4}\eta_i^4\right) + \gamma\sum_{i=1}^{p}\sum_{j\neq i}^{p}\eta_i^2\eta_j^2 \quad (8)$$

where α, β and γ are positive constants. For simplicity, let us assume $\alpha = 1$ and $\beta = 1$. In this case, it can be easily seen that each term in the first summation in the right-hand side of equation (8) is a double-well potential with the wells located at $\eta_i = -1$ and $\eta_i = 1$, and with a well-depth of -0.25. However, the first summation alone cannot satisfy our requirement since it will have a total number of 2^p minima located at the positions where each η_i is either equal to 1 or -1, such as $(\eta_1, \eta_2, \ldots, \eta_p) = (1, 1, \ldots, 1)$. Therefore, the cross terms were added to equation (8) as a double summation. With a proper choice of γ, the potential function can satisfy our requirement. To see how to choose γ, let us rewrite expression (8) as follows:

$$f_0(\eta_1, \eta_2, \ldots, \eta_p) = -\frac{\alpha}{2}\sum_{i=1}^{p}\eta_i^2 + \frac{\beta}{4}\left(\sum_{i=1}^{p}\eta_i^2\right)^2 + \left(\gamma - \frac{\beta}{2}\right)\sum_{i=1}^{p}\sum_{j\neq i}^{p}\eta_i^2\eta_j^2. \quad (9)$$

Now it is quite clear that if $\gamma = \beta/2$, f_0 has infinitely degenerate minima for any $p > 1$, located at the loci described by

$$\sum_{i=1}^{p}\eta_i^2 = \alpha/\beta = 1.$$

For $p = 2$, these loci form a circle, for $p = 3$ they form a sphere, etc. For $\gamma < \beta/2$, f_0 has 2^p minima with each η_i being either equal to 1 or -1. For $\gamma > \beta/2$, f_0 has $2p$ minima located at $(\eta_1, \eta_2, \ldots, \eta_p) = (1, 0, \ldots, 0)$, $(0, 1, \ldots, 0)$, $\ldots$, $(0, 0, \ldots, 1)$, $(-1, 0, \ldots, 0)$, $(0, -1, \ldots, 0)$, $\ldots$, $(0, 0, \ldots, -1)$. Therefore, γ has to be greater than $\beta/2$ in order for f_0 to satisfy our requirement. In modelling grain growth, each of the $2p$ minima represents a specific crystallographic orientation of grains. An example of the free energy surface with $p = 2$ and $\gamma = 1$ is shown in Fig. 3 in which there are four minima located at $(\eta_1, \eta_2) = (1, 0), (0, 1), (-1, 0)$ and $(0, -1)$.

Using the expression for f_0 given in (8) and then substituting the total free energy F (equation (2)) into equation (4), we obtain the kinetic equations,

$$\frac{\partial \eta_i}{\partial t} = -L_i\left(-\alpha\eta_i + \beta\eta_i^3 + 2\gamma\eta_i\sum_{j\neq i}^{p}\eta_j^2 - \kappa_i\nabla^2\eta_i\right), \quad i = 1, 2, \ldots, p. \quad (10)$$

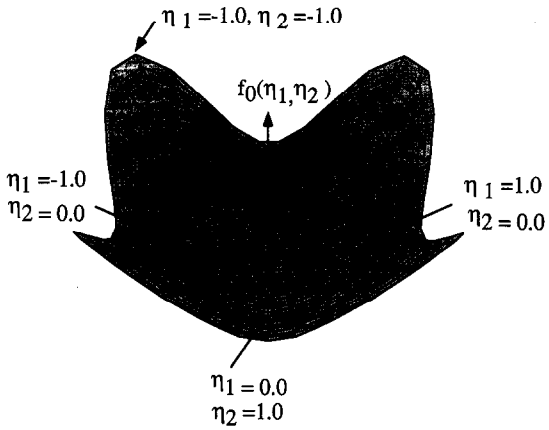

Fig. 3. Free energy density surface with two orientation variables with the cross term $\gamma = 1.0$.

5. NUMERICAL SOLUTION TO THE KINETIC EQUATIONS

In order to simulate the grain growth kinetics, the set of kinetic equations (10) have to be solved numerically by discretizing them in space and time. In our simulation, the Laplacian is discretized by the following equation,

$$\nabla^2\eta_i = \frac{1}{(\Delta x)^2}\left[\frac{1}{2}\sum_j (\eta_j - \eta_i) + \frac{1}{4}\sum_k (\eta_k - \eta_i)\right] \quad (11)$$

where Δx is the discretizing grid size, j represents the first nearest neighbours of site i, and k represents the second nearest neighbours. For discretization with respect to time, we employed the simple explicit Euler equation,

$$\eta_i(t + \Delta t) = \eta_i(t) + \frac{d\eta_i}{dt} \times \Delta t \quad (12)$$

where Δt is the time step for integration. For a given initial distribution of η_i, which describes the initial grain structure, the temporal and spatial evolution of the microstructure can be obtained by numerically solving equation (10). A grain growth simulation can be started in two different ways: (1) inputting a pre-defined initial microstructure, or (2) generating a liquid phase by assigning small random values to all field variables, e.g. between -0.001 and 0.001, and then allowing crystallization to occur, which will generate a fine grain microstructure. All the statistical information about the grain structure at a given time, the average growth rate, topological changes of each individual grains, etc. can be obtained from the computer generated microstructures.

6. RESULTS AND DISCUSSION

All the results reported in this paper are in 2-D systems and we assumed the following numerical values for the parameters in the kinetic equations: $\alpha = 1.0$, $\beta = 1.0$, $\gamma = 1.0$, and $\kappa_i = 2.0$, and $L_i = 1.0$ for $i = 1$ to p. The grid size along both Cartesian coordinate axes, Δx, was chosen to be 2.0, and the time step for integration, $\Delta t = 0.25$. Periodic boundary conditions were applied. Two different sizes of computational cells, 512×512 and 1024×1024 grid points, were chosen for comparing the size dependence of grain growth. The initial condition is specified by assigning small random values to all field variables at every grid point, e.g. $-0.001 < \eta_i$ (for i) < 0.001, simulating a liquid. All kinetic data were obtained by averaging over several independent runs starting with different initial conditions (produced from a random number generator with different seeds) for the orientation field variables. A typical simulation with 512×512 grid points and 8000 time steps requires about 2 h in a Cray C-90.

6.1. *Microstructure evolution*

To visualize the microstructure evolution using the orientation field variables, the following function is defined:

$$\varphi(r) = \sum_{i=1}^{p} \eta_i^2(r). \quad (13)$$

Function $\varphi(r)$ has the value, 1.0, within grains and significantly smaller values at grain boundaries. If these values are displayed by grey-levels with low and high values represented by black and white respectively, the bright regions will be grains and dark lines will be grain boundaries in a microstructure. An example of microstructural evolution using a 512×512 cell with 36 field variables is shown in Fig. 4. Since the initial values for η_i are essentially zero, the very early stage of the simulation corresponds to crystallization, i.e. the growth of η_i values at different locations driven by the bulk free energy change. A well defined grain structure is formed after a short time, about 200 time steps, when essentially all the bulk driving force has been consumed. Further microstructure evolution is driven by the excess free energies associated with the grain boundaries, resulting in an increase of the overall microstructure scales or grain size (Fig. 4). The detailed topological changes of individual grains will be discussed later.

6.2. *Grain growth exponent*

The area of each grain at a given time step is directly calculated from the microstructure by counting the number of grid points within a grain, and grain size R is obtained from the area A by assuming a circular shape for all grains, therefore, $A = \pi R^2$. The average grain radius at a given time step is then obtained by averaging over all the grains in a system. The initial number of grains immediately after crystallization is about 3000 in a 512×512 cell, and there are about 200 grains left after 10 000 time steps.

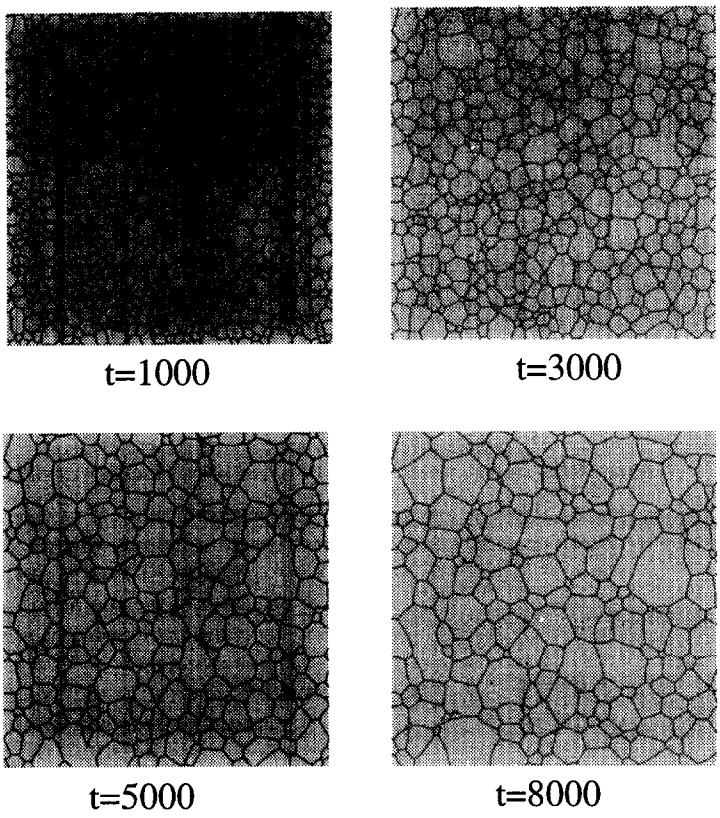

Fig. 4. The microstructural evolution in the 512 × 512 system with 36 orientation variables.

The average grain radius as a function of time for the 512 × 512 system is shown in Fig. 5. The data were then fitted to the equation $\bar{R}_t^m - \bar{R}_0^m = kt$ by a multi-parameter nonlinear least-square fitting routine to extract growth exponent m and coefficient k. The data from the initial stage, about 500 to 1000 time steps, were removed before the fitting. The growth exponent, m, is shown to be almost exactly 2.0.

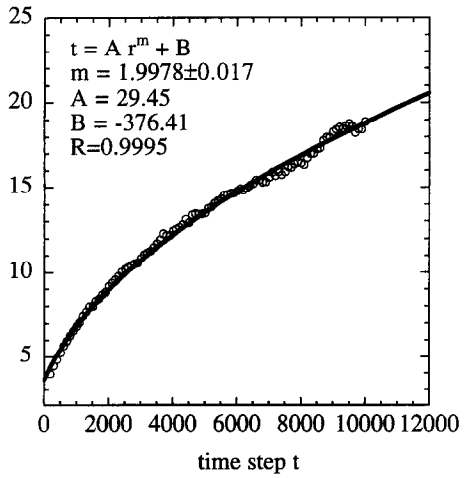

Fig. 5. The time dependence of average grain size in the 512 × 512 system with 36 orientation variables. Data are fitted into equation $\bar{R} = At^m + B$ (solid line).

6.3. *Grain size distribution*

The grain size distribution obtained from the 512 × 512 system is shown in Fig. 6. There have been several functions proposed to describe the grain size distribution [2, 4, 6, 7]. We attempted to fit the grain size distribution from our simulation to two theoretical distributions, the log-normal function and the generalized Louat's function [6, 7, 16].

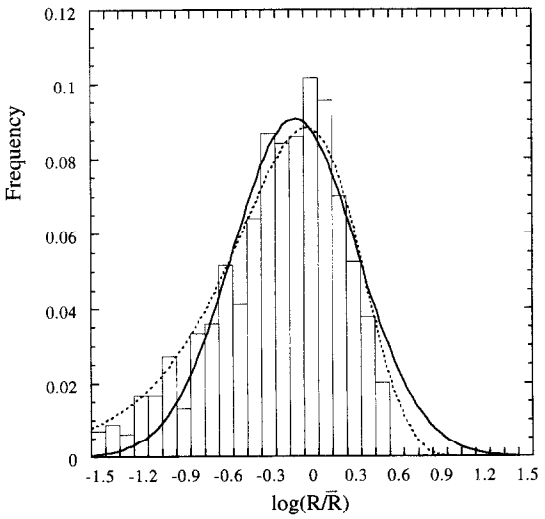

Fig. 6. Size distribution in the 512 × 512 system compared with log-normal function (solid line) and Louat's function (dashed line).

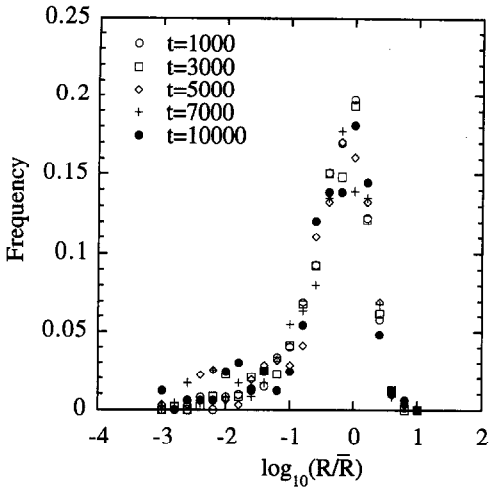

Fig. 7. The time dependence of grain size distribution in the 512 × 512 system with 36 orientation variables.

The log-normal distribution may be written as:

$$F(x) = \frac{1}{\sqrt{2\pi\sigma^2}} \exp\left(\frac{-(x-x_0)^2}{2\sigma^2}\right) \qquad (14)$$

where $x = \log(R/\bar{R})$, x_0 is the mean of x, and σ is the standard deviation of the distribution. The generalized Louat's function [4, 15] has a form:

$$F(x) = 2\alpha x \exp(-\alpha x^2) \qquad (15)$$

where α is an adjustable parameter. The log-normal and generalized Louat's distribution functions were fitted into simulation data by a multi-parameter nonlinear least-square fitting routine (Fig. 6). It can be seen that the log-normal distribution fits simulation data fairly well near the average size region, but there are large deviations in the small size and large size regions. Moreover, the log-normal distribution in logarithmic plot is symmetric with tails extending to $\pm\infty$ whereas the simulation data are asymmetric and have cut-off at the large size region. The Louat's distribution function agrees reasonably well with simulation data in the entire region and an upper cut-off is obtained at about $\log_{10}(R/\bar{R}) = 0.85$. However, the maximum of Louat's function is considerably lower than that of the simulation data even though it appears at the same position. While the majority of the above results agree with those reported from Monte Carlo simulations [14, 16], the upper cut-off limit is different.

The time dependence of the grain size distribution for a 512 × 512 system with 36 field variables is shown in Fig. 7 for different time steps. It was found that the size distributions are essentially time-independent and self-similar after a short transient time, indicating that the system has reached the dynamic steady state or scaling region.

It should be cautioned that our results were obtained from 2-D simulations. As shown in [16], Louat's distribution function is a better fit to the grain size distribution obtained in 2-D computer simulations, whereas the log-normal distribution provides a better fit to the grain size data calculated from the grain volume in a 3-D simulation instead of from 2-D cross-sections.

It may also be pointed out that the shape of the grain size distribution depends on how we bin the data unless the frequencies obtained from different bins are normalized by their respective total areas under the curves. Therefore, it is important to use the normalized grain size distribution for comparing results from different sources or obtained with different bins.

6.4. *Effect of the number of field variables*

Since the total number of different orientations in a real system is infinite, whereas only a finite number can be simulated in a computer, it is important to study the effect of the number of field variables on the microstructural evolution and grain growth kinetics. We again chose a 512 × 512 cell. It was found that, for small p, microstructural coarsening is dominated by coalescence between grains with the same orientation. As p increases, the possibility of grain coalescence decreases and the coarsening is dominated by grain growth, i.e. the larger grains grow by consuming smaller ones.

The time dependencies of the average grain area on the number of field variables are shown in Fig. 8. It can be seen that the mean grain areas increase linearly with time for all cases, implying a parabolic growth law. The slopes of the curves, which are proportional to the kinetic coefficient k, decrease as p increases. For high values of p, such as $p = 36$ and 50, the two curves are very close to each other. The grain growth exponent m and kinetic coefficient k are plotted against the number of field variables in Fig. 9. It is found (Fig. 9(a)) that the growth exponent m is equal

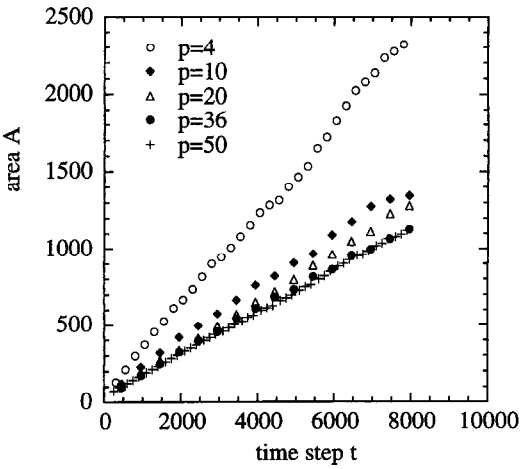

Fig. 8. The time dependence of average grain area in the 512 × 512 system with different numbers of orientation variables.

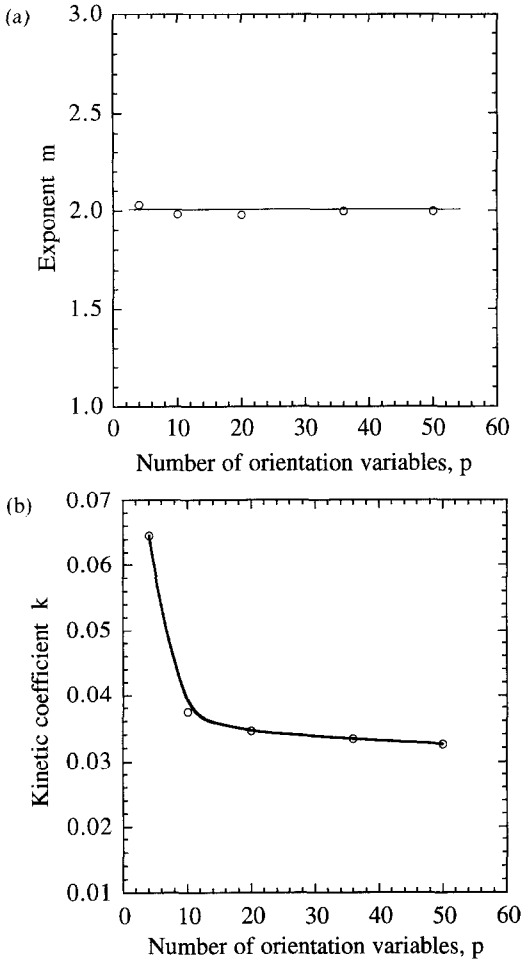

Fig. 9. The dependence of growth exponent m and coefficient k on the number of orientation variables in the 512 × 512 system: (a) growth exponent m; (b) coefficient k.

to 2.0 with small statistic errors for all cases and does not change with p. The value of k decreases rapidly as a function of p at small p values ($p < \sim 10$) (Fig. 9(b)) and it changes much slower at large p ($p \geqslant 20$). This indicates that it is possible to use a finite but large number of field variables to study grain growth kinetics.

The influence of the number of field variables on grain size distributions is shown in Fig. 10, in which the grain size distribution for each p is plotted with frequency of occurrence against the logarithm of the normalized grain size, $R/\bar{R}$. The height of the peak in the distribution for $p = 4$ is clearly lower than those for large p, and the position of the peak for $p = 4$ is located at smaller sizes than for large p. This indicates that the microstructure for $p = 4$ contains some large grains due to coalescence and many small grains with the population dominated by small grains. At large p, e.g. $p = 36$ and $p = 50$, the positions of peaks in the distribution almost coincide with the average size and the shapes of distributions are asymmetric. There is no distinguishable difference between distributions for $p = 36$ and 50.

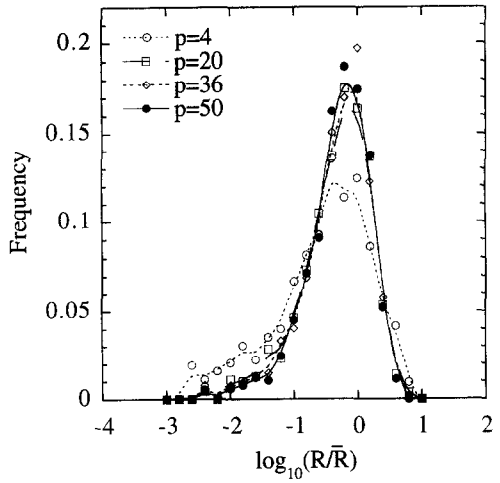

Fig. 10. The influence of the number of orientation variables on the grain size distributions in the 512 × 512 system.

6.5. *Effect of computational cell size*

The effect of system size on grain growth kinetics and grain size distribution was studied by choosing two different sizes, 512 × 512 and 1024 × 1024 grid points, both with 36 field variables. For 1024 × 1024, the initial number of grains immediately after crystallization is about 10 000 compared with about 3000 for a 512 × 512 system. In the 1024 × 1024 system, there are about 500 grains left after 15 000 time steps, compared with about 200 after 10 000 time steps for 512 × 512. The grain growth exponent and kinetic coefficient obtained in the 1024 × 1024 system are essentially identical to those from the 512 × 512 system, indicating that, with the specific parameters used in this work, 512 × 512 grid points are sufficient for obtaining the growth kinetics. The size distributions calculated from the two different systems at the same time step are compared in Fig. 11. It can be seen that the shapes of the distributions are very similar.

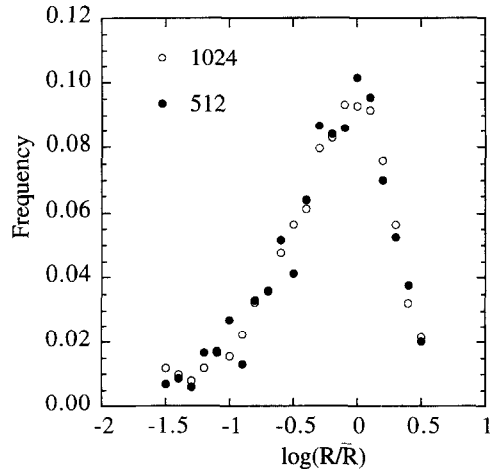

Fig. 11. Comparison of grain size distributions in the 512 × 512 and 1024 × 1024 systems ($p = 36$).

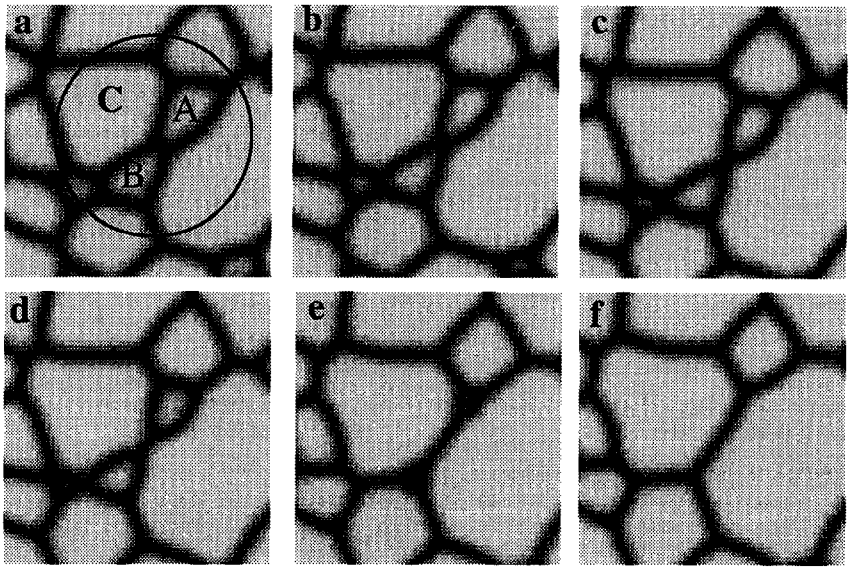

Fig. 12. *In situ* observation of neighbour switching and 3-sided grain annihilation.

The grain size distributions obtained in this model seem to agree well with large scale Monte Carlo simulations [33]. It should be pointed out that an upper grain size limit is observed to be near $\log_{10}(R/\bar{R}) = 0.85$ in this work, which is close to the result of the large scale Monte Carlo simulation [33], but it is different from previous Monte Carlo simulation results, in which an upper limit about $\log_{10}(R/\bar{R}) = 0.52$ was reported [15].

6.6. *Local topological changes*

Based on the behaviour of individual grains and the uniform boundary model, Mullins and von Neumann [34, 35] gave a correlation between grain growth kinetics and the topological class of individual grains:

$$\frac{dA}{dt} = k_N(N - 6), \tag{16}$$

where A is the grain area, N the topological class of the grain, and k_N is a kinetic constant. According to this equation, grains with sides more than six will grow while grains with sides less than six will shrink. Smith [36] pointed out that the shrinkage of a 5-sided grain must transform to a 4-sided and then to a 3-sided grain before it disappears. However, recent experimental observation on 2-D grain growth in succinonitrile thin films [29] showed that 4-sided and 5-sided grains can directly disappear without transforming to 3-sided.

Since we are only interested in the local topological changes of individual grains during shrinking, a smaller system with 128×128 grid points was employed. After 2000 time steps, at which time well defined grain structures were formed, some grains were chosen and their topological evolutions were monitored for every 10 time steps. We observed two different types of topological transformations during the disappearance of a grain: (1) neighbour switching, which occurs when the length of a grain boundary decreases to zero and results in the formation of unstable four-grain junctions, which quickly split into two trijunctions and a new grain boundary; (2) the direct vanishing of grains with $N < 6$.

An example of neighbour switching and then vanishing of 3-sided grains is shown in Fig. 12. In this figure, two small grains with four and five sides (labelled as A and B) are shrinking. When the boundary length between these two grains reduces to zero, a neighbour switching event occurs and the two grains decrease their topological class by 1 while two larger neighbour grains increase by one. The resulting 3-sided grain later disappears and a trijunction is formed, while the two larger grains retain their own topological classes. It should be pointed out that vanishing of 3-sided grains is rarely observed during microstructural evolution, especially in the later stage of grain growth. This result is consistent with experimental observations in SCN [29]. The local topology change for grains with $N > 6$ can be very complicated because more than one neighbour grain may disappear within a short time. In this example, the large grain (labelled as C) changed its topological class from 8 to 9, and from 9 to 10, and then jumped back to 8 due to the vanishing of two small grains at the same time.

Figure 13 is another example showing rather different characteristics in the local topological changes of a grain. It can be seen in Fig. 13 that a 4-sided grain stays in its topological class until it disappears. As a result, a four-grain junction is formed and it quickly splits into two trijunctions because of its instability. It is interesting to notice that the formation of this four-grain junction is not due to neighbour switching but, instead, the direct vanishing of a 4-sided grain. It was also observed that

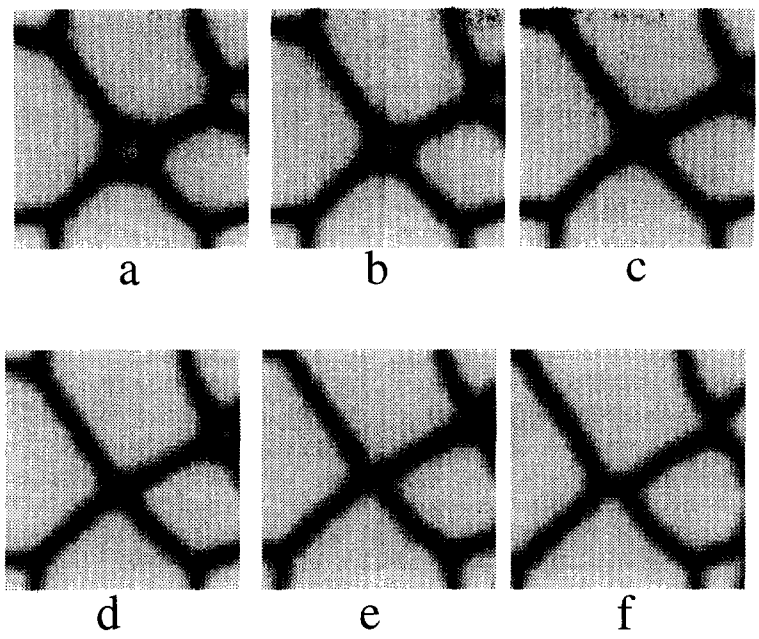

Fig. 13. *In situ* observation of 4-sided grain annihilation.

an elongated 4-sided grain can undergo vanishing directly when its width decreases to zero. In this case, no four-grain junction will form after its vanishing. From the careful examinations of the simulation results, it seems that the direct vanishing of 4-sided grains is quite common. Actually it is a dominant mechanism rather than an exception during grain growth, especially during late stages of grain growth. It is found that before 4-sided grains directly disappear, they become a disordered region whose width is of the order of the grain boundary width and whose boundaries with neighbouring grains are not well defined.

In addition to 4-sided grains, we also examined the topological changes of some 5-sided grains (Fig. 14). Similar to the 4-sided, 5-sided grains can directly vanish without losing sides. However, no five-grain junctions were observed. For example, the 5-sided grain in Fig. 14 directly disappears forming three trijunctions while two neighbouring grains lose one side each. Again, before this grain disappears, it transforms to a region of disordered material. It should be emphasized that, in this computer simulation, the majority of 5-sided grains vanish through changing topological class to 4-sided by neighbour switching.

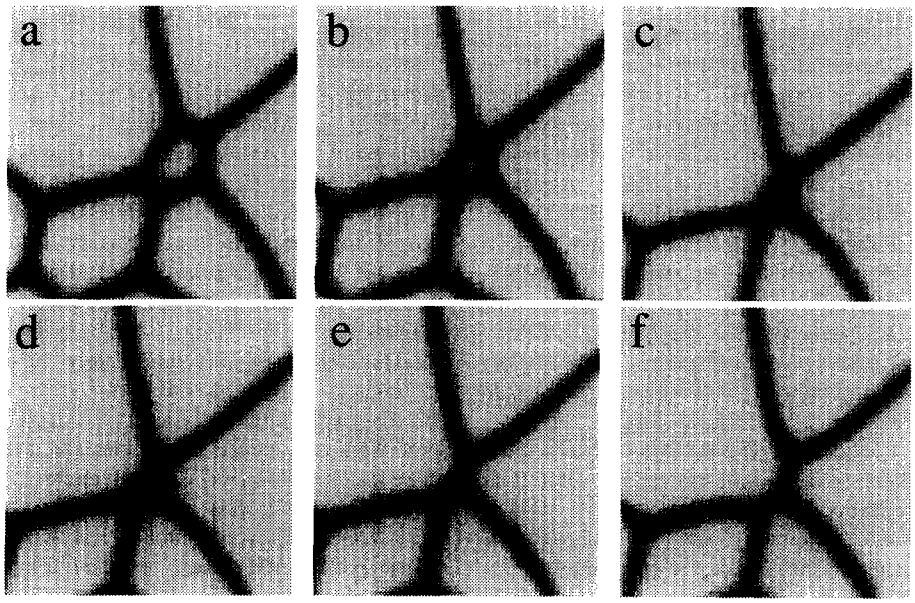

Fig. 14. *In situ* observation of 5-sided grain annihilation.

In summary, we observed four different kinds of topological events during the disappearance of a grain: direct vanishing of 3-sided grains, 4-sided grains, and 5-sided grains, and neighbour switching. Neighbour switching and direct vanishing of 4-sided grains occur most often, especially in late stages of grain growth. Direct vanishing of a 4-sided grain may result in either a four-grain junction or a grain boundary between two neighbouring grains. Five-grain junctions are never observed in the simulation. The most probable explanation for this phenomenon is that the balance of surface tension among the neighbour grains prohibits the formation of five-grain junctions because of the asymmetric feature. Most of these phenomena seem to agree with experimental observations of grain growth in SCN thin-films [29]. However, it should be noted that these 2-D topological features may not be observed in a cross-section of 3-D samples because the local topology equilibrium requirements are different for 2-D and 3-D. It should also be pointed out that in the diffuse-interface field model, when the size of a grain becomes comparable with the grain boundary width, the grain is not well defined any more. Essentially, a region of disordered material is formed, whose size is comparable with the grain boundary width, immediately before a grain completely disappears. We argue that this should also be the case in real systems in which grain boundaries have a finite width and we claim that sharp-interface models are inappropriate for describing grains with sizes close to the boundary width.

7. ASSESSMENT OF THE MODEL

All previous models on grain growth are based on the sharp-interface description of grain boundaries although, as a matter of fact, the Potts model at finite temperatures produces rough or diffuse interfaces. There are several advantages of the diffuse-interface model over traditional sharp-interface models in modelling grain growth. One of the main advantages is the fact that one does not have to track explicitly the positions of grain boundaries since locations of grain boundaries are implicitly defined by the regions where the gradients of field variables are not zero. Secondly, in the diffuse-interface field model, it is straightforward to describe long-range diffusion—which takes place, for example, during solute segregation and second-phase precipitation at grain boundaries in a polycrystalline material—by coupling the kinetic equations for the orientation field variables with the Cahn–Hilliard diffusion equation for composition [25, 26], whereas it is very difficult to incorporate long-range diffusion in sharp-interface models. The lattice anisotropy effect which exists in the Potts model is almost non-existent if there are enough grid points to resolve the grain boundaries.

Like all other models, there are problems associated with the diffuse-interface field model. For example, although grain boundaries in real materials have a finite thickness (a few lattice parameters in very pure metals to a few hundred angstroms in ceramics), this thickness is much smaller than the typical grain size (a few micrometres) studied experimentally except in nanocrystalline materials. Therefore, we have to deal with two quite different length scales if we want to apply the model to grain growth kinetics in polycrystalline materials with grain sizes on the order of micrometres.

The problem with two very different length scales is not associated with the diffuse-interface formulation itself, but with the numerical computation. For example, if we employ five grid points to resolve a grain boundary of width about 20 Å, a grain size of 1 μm will require about 250 grid points across the diameter. In order to obtain the grain growth kinetics, we will need at least several thousand, to tens of thousands, of grains for good statistics, which translates to a number of grid points of the order of 100 billion, which is impossible to handle with today's supercomputers. However, we claim that this is not a very serious problem for most of our purposes in studying grain growth and this problem is non-existent for nanocrystalline materials.

First of all, many analytical theories and computer simulations, including our present work, show evidence that the microstructure scales, i.e. after a microstructure reaches the scaling region, the average grain size as a function of time can be described by a time exponent while the grain size distribution is independent of time. The important implication of scaling is that we can use the information that we obtained from microstructures with much smaller scales to predict the microstructure features with a much larger scale which occur at a later time. This means we do not have to model microstructures with larger length scales as long as the microstructures obtained from the computer simulation are already in the scaling region.

Secondly, for the purpose of modelling grain growth, we can view the migration of a diffuse grain boundary as an approximation to that of a sharp grain boundary. The validity of this argument is illustrated in Fig. 15 in which the radius of a circular grain with several different boundary thicknesses is plotted together with the analytical solution as a function of time. The analytical solution was obtained from the analytical expression (7) which assumes the grain size is much larger than the boundary thickness, and others were obtained from the numerical solution using two orientation field variables with different boundary widths. As can be seen from the plots, the agreement between the analytical solution and data of curve 1 ($0.25f$) is surprisingly good, even in the region that the grain size is very small, which implies that the motion of a diffuse grain boundary is an excellent approximation to that of a sharp boundary. However, as discussed by many others in the context of the phase-field

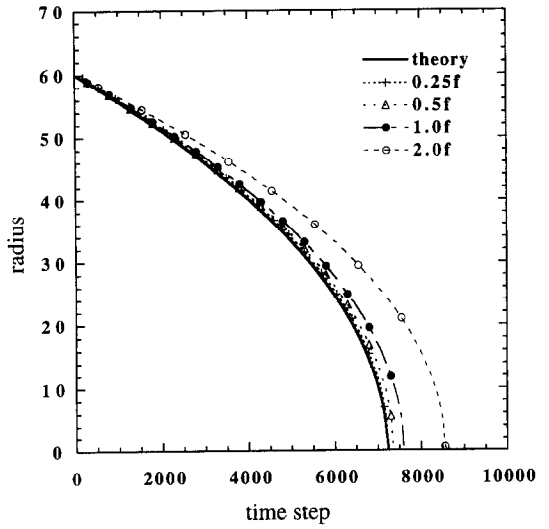

Fig. 15. The time dependence of the radius of a circular grain in an infinite matrix. Comparing the analytical solution (equation (7)) with simulations of different boundary widths obtained by multiplying the local free energy density function, f_0, with different coefficients 0.25, 0.5, 1.0 and 2.0, while keeping the gradient coefficient κ constant.

model for solidification [32], in order to have a good agreement between the diffuse-interface computation and analytical solution in the sharp-interface limit, a sufficient number of grid points is necessary for resolving the grain boundary thickness. For example, by changing the well depth in the local free energy function, we can change the grain boundary thickness with respect to the grid size (Fig. 15). On the other hand, according to equation (7), changing the well depth should not alter the boundary migration velocity. Figure 15 shows that the boundary should be sufficiently wide in the simulation, or there should be enough grid points across the boundary, in order for the boundary velocity not to depend on the well depth in the free energy function. However, it may be noted that although some deviations in the kinetic coefficients k may be introduced compared with the analytical solution, if not enough grid points are used to resolve the boundaries, the radius of the circular domain still varies parabolically as a function of time. The grain growth kinetics discussed above were obtained using the set of parameters which correspond to curve 4 ($2.0f$) in Fig. 15 in order to obtain a large number of grains and good statistics, and therefore, some deviations in the kinetic coefficients k are introduced simply because of not enough grid points to resolve the grain boundary thickness. Nevertheless, this difference will not change the main conclusions of our discussion.

8. CONCLUSIONS

We have demonstrated that the diffuse-interface field model is a very powerful alternative to sharp-interface models for studying grain growth. The grain growth exponent m is 2 and independent of the number of field variables, whereas the kinetic coefficient depends on the number of field variables although it varies slowly for numbers of field variables greater than about 10. The grain size distribution obtained in our 2-D simulation is shown to fit reasonably well to the Louat's function but not as well to the log-normal distribution. Using a particular example of a circular grain, it is found that, with a sufficient number of grid points to resolve a grain boundary in the simulation, the boundary migration velocity is very close to that predicted by the analytical solution obtained assuming the boundary thickness is much smaller than the grain size, and independent of the particular free energy density function employed in the numerical solution. Contrary to the general belief that 4- and 5-sided grains have to transform to 3-sided before their disappearance in 2-D grain growth, we found evidence that 4-sided and 5-sided grains may transform to a disordered region and directly vanish.

Acknowledgements—The work is supported by the National Science Foundation under the grant number DMR 93-1898 and the simulations were performed at the Pittsburgh Supercomputing Center. We thank Mr Wei Yang for providing the code of grain size calculation.

REFERENCES

1. H. V. Atkinson, *Acta metall.* **36,** 469 (1988).
2. D. Weaire and J. A. Glazier, *Materials Science Forum*, vol. 94–96, p. 27, Pt. 1 (1992).
3. R. J. Brook, in *Ceramic Fabrication Processes* (edited by F. F. Y. Wang), p. 331. Academic Press, New York (1976).
4. M. Hillert, *Acta metall.* **13,** 227 (1965).
5. J. E. Burke and D. Turnbull, *Prog. Metal Phys.* **3,** 220 (1952).
6. P. Feltham, *Acta metall.* **5,** 97 (1957).
7. N. P. Louat, *Acta metall.* **22,** 721 (1974).
8. D. Weaire and F. Bolton, *Phys. Rev. Lett.* **65,** 3449 (1990).
9. D. Weaire and J. P. Kermode, *Phil. Mag. B* **47,** L29 (1983).
10. D. Weaire and H. Lei, *Phil. Mag. Lett.* **62,** 47 (1990).
11. R. L. Fullman, in *Metal Interfaces*, p. 179. American Society for Metals, Cleveland (1952).
12. K. Kawasaki, T. Nagai and K. Nakashima, *Phil. Mag. B* **60,** 399 (1989).
13. C. V. Thompson, H. J. Frost and F. Spaepen, *Acta metall.* **35,** 887 (1987).
14. M. P. Anderson, D. J. Srolovitz, G. S. Grest and P. S. Sahni, *Acta metall.* **32,** 783 (1984).
15. D. J. Srolovitz, M. P. Anderson, P. S. Sahni and G. S. Grest, *Acta metall.* **32,** 793 (1984).
16. M. P. Anderson and G. S. Grest, *Phil. Mag. B* **59,** 293 (1989).
17. S. Kumar, S. K. Kurtz, J. R. Banavar and M. G. Sharma, *J. Stat. Phys.* **67,** 523 (1992).
18. S. K. Kurtz and F. M. A. Carpay, *J. Appl. Phys.* **51,** 5125 (1980).
19. V. E. Fradkov, A. S. Kravchenko and L. S. Shvindlerman, *Scripta Met.* **19,** 1291 (1985).
20. C. W. J. Beenakker, *Phys. Rev. A* **37,** 1697 (1988).
21. M. Marder, *Phys. Rev. A* **36,** 438 (1987).

22. N. Rivier, *Phil. Mag.* **B47,** L45 (1983).
23. L.-Q. Chen, *Scr. Metall. et Mater.* **32,** 115 (1995).
24. L.-Q. Chen and W. Yang, *Phys. Rev. B* **50,** 15 752 (1994).
25. D. Fan and L.-Q. Chen, in *Proceedings of the American Ceramic Society 1995 Annual Meeting*, Cincinnati, Ohio (1995).
26. L.-Q. Chen and D. Fan, *J. Am. Ceram. Soc.*, **79,** 1163 (1996).
27. S. M. Allen and J. W. Cahn, *Acta Metall.* **27,** 1085 (1979).
28. V. E. Fradkov, M. E. Glicksman and K. Rajan, in *Modeling of Coarsening and Grain Growth* (edited by S. P. Marsh and C. S. Pande), p. 183. TMS (1993).
29. M. Palmer, K. Rajan, M. Glicksman, V. Fradkov and J. Nordberg, *Metall. and Mater. Trans. A* **26A,** 1061 (1995).
30. J. W. Cahn and J. E. Hilliard, *J. Chem. Phys.* **28,** 258 (1958).
31. Y. Oono and S. Puri, *Phys. Rev. Lett.* **58,** 836 (1987).
32. R. Kobayashi, *Experim. Math.* **3,** 59 (1994), and references therein.
33. E. A. Holm, private communication.
34. W. W. Mullins, *J. Appl. Phys.* **27,** 900 (1956).
35. J. von Neumann, *Metal Interfaces*, p. 108. ASM, Cleveland, OH (1952).
36. C. S. Smith, *Trans. Am. Soc. Metals* **45,** 533 (1953).